AAS 17-320

RAPID CHARGED GEOSYNCHRONOUS DEBRIS PERTURBATION MODELING OF ELECTROMAGNETIC DISTURBANCES

Joseph Hughes* **and Hanspeter Schaub†**

Charged space objects experience small perturbative torques and forces from their interaction with Earth's magnetic field. These small perturbations can change the orbits of lightweight, uncontrolled debris objects dramatically even over short periods. This paper investigates the effects of the isolated Lorentz force, the effects of including or neglecting this and other electromagnetic effects in a full propagation, and then analyzes for which objects electromagnetic effects have the most impact. It is found that electromagnetic forces have a negligible impact on their own. However, if the center of charge is not collocated with the center of mass, electromagnetic torques are produced which due impact the attitude, and thus the translation through the strong solar radiation pressure perturbation. The objects for which electrostatic torques have the most influence are charged above the kilovolt level, have a difference between their center of mass and center of charge, have highly attitude-dependent cross-sectional area, and are not spinning stably about an axis of maximum inertia. Fully coupled numerical simulation illustrate the impact of electromagnetic disturbances through the solar pressure coupling.

INTRODUCTION

The two-body equations of motion are not sufficient to describe the orbital motions of all objects. At low altitudes, Earth's spherical gravity and drag strongly perturb certain orbits. Further out in Geosynchronous (GEO) orbit, all objects are perturbed by lunar and solar gravity, and some High Area-to-Mass (HAMR) objects are strongly perturbed by Solar Radiation Pressure (SRP).[1]

However, SRP is not sufficient to explain the motions of all HAMR GEO objects. The 28th International Symposium for Space Technologies and Sciences held in London in June 2011 identified this issue. In particular, Professor Schildknecht discussed that families of HAMR objects have been identified whose mean motion changes remain very small, while the orbital angular momentum of these objects changes significantly with eccentricities varying up to 0.7. Additionally, Wiesel recently reported in Reference 2 some near-GEO debris objects which appear to accelerate *towards* the sun during the propagation interval, which is impossible with SRP. One possible source of this discrepancy is that these objects may be interacting with Earth's magnetic field.

Some of these objects that are hard to model are thought to be torn-off pieces of Multi-Layer Insulation (MLI).[3] Samples returned from the Hubble Space Telescope showed cracks in areas of constrained loading, and had a tendency to curl up when peeling off.[4] MLI may peel off of GEO spacecraft, and could charge to very high potentials during geomagnetic storms.[5] This charging

*Graduate Research Assistant, Aerospace Engineering Sciences, University of Colorado.

†Alfred T. and Betty E. Look Professor of Engineering, Associate Chair of Graduate Affairs, Department of Aerospace Engineering Sciences, University of Colorado, 431 UCB, Colorado Center for Astrodynamics Research, Boulder, CO 80309-0431. AAS Fellow

causes a translational Lorentz force, and may cause a significant electrostatic torque depending on the relative distance between the center of charge and center of mass. Additionally, if the object is rotating relative to an external magnetic field it will experience a eddy current torque, which acts to slow the rotation.

Früh et al. where the first to publish results modeling the electrostatic charging effects on HAMR objects.[6] This initial work adds the Lorentz force and eddy torque to the more standard list of perturbations for a HAMR plate. Including these two new effects changes the orbit by nearly a tenth of a degree in inclination and 0.002 in eccentricity after only 12 hours. Paul et al.[7] modeled a sphere for which torques are not included and found much less dramatic results. Reference 8 considered a flat plate similar to Früh et al., but added electrostatic torques as a perturbation and found that considering these perturbations caused large orbital impacts.

This paper examines under what conditions the electrostatic charging or the Eddy current need to be included, and how they impact the resulting orbital motion. First a charged sphere is studied using a Gaussian variation of parameters and acceleration magnitude to find the size regime where the Lorentz force will matter and how the orbit will change. Next, different propagators which include or neglect certain perturbations are used for a HAMR plate similar to the one used by Früh et al. to determine the coupled effect of these perturbations. Next, Monte Carlo analysis is used to investigate whether these findings are significant considering the spread due to attitude variation. The change in both ECI position and classical orbital elements are considered. Finally, the objects and obit scenarios are found for which electrostatic torque will matter the most.

OVERVIEW OF ELECTROSTATIC FORCE AND TORQUE ESTIMATION

There are many methods for predicting the electrostatic force and torque on conductors in external fields. They vary in computational speed, accuracy, and analytic predictive ability.

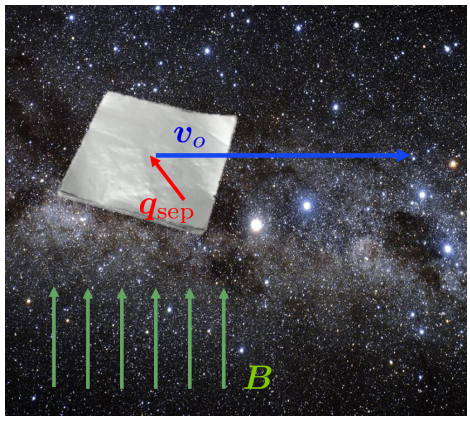

Figure 1. Flat External Field Configuration

Multi-Sphere Method

The Multi-Sphere Method (MSM) is an elastance-based method for predicting the force and torque on conductors.[9] Unlike the Method of Moments or Finite Element Method (FEM), MSM uses nodes of tunable size and location to match the force and torque predicted by a higher-fidelity solver such as FEM software. This allows MSM to predict forces and torques on conductors very

quickly to allow for faster-than-realtime simulations and control. MSM divides into Volume MSM (VMSM) and Surface MSM (SMSM).[10] VMSM uses relatively few (1-3) spheres placed in the volume of the object being modeled, while SMSM use a large number (50-500) of spheres placed equidistantly on the surface of the body. The radii of each sphere is set so that the self capacitance of the SMSM model matches the self capacitance of the actual object. SMSM is much easier to set up, but slower to run than VMSM.

In this analysis, MSM is not used for electrostatic force and torque computation. Rather, SMSM models are used to make parameters needed for the Appropriate Fidelity Measures method which is used to compute force and torque. A completed SMSM model with correctly sized spheres and color representing the charge each sphere holds is shown in Fig. 2. As is expected, more charge accumulates near the corners of the plate. The center of charge is located in the center of area, but the center of mass, about which torques are taken, is removed by 2 mm in both $\hat{\boldsymbol{x}}$ and $\hat{\boldsymbol{y}}$.

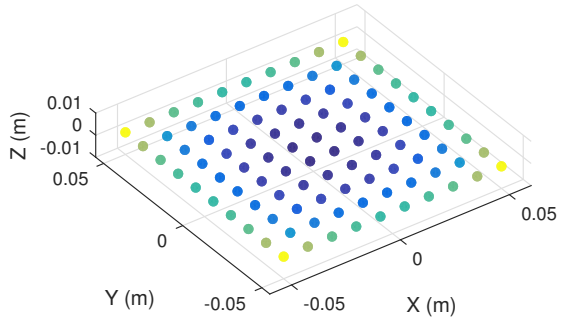

Figure 2. Flat plate modeled with SMSM, color indicates charge

Appropriate Fidelity Measures

The Appropriate Fidelity Measures (AFM) method is a closed-form method for predicting electrostatic force and torque based on a truncated expansion.[11] This method is very similar to a multipole expansion,[12] and gives analytic results which makes it very suitable for control. In a locally flat field (such as Earth's magnetic field at GEO), there is no expansion to truncate, and the AFM results match alternate formulations.[13,14] Additionally, if an MSM model is used to make the parameters used in AFMs, the differences between force and torque computed by MSM and AFMs differ by numerical precision.

Force and Torque Estimation The force and torque on a charged conductor are the result of the Lorentz field and the ambient electric field: $\boldsymbol{A} = \boldsymbol{E} + \boldsymbol{v} \times \boldsymbol{B}$, where $\boldsymbol{A}$ is the total field, $\boldsymbol{E}$ is the environmental electric field, $\boldsymbol{B}$ is the environmental magnetic field, and $\boldsymbol{v}$ is the velocity of the spacecraft relative to the magnetic field, which co-rotates with Earth. Although electric fields are observed in L shells similar to GEO,[15] they are typically oscillatory and would not change an orbit, although they may be able to cause shape changes in flexible materials.

The differential force on a differential charge moving at $\boldsymbol{v}$ subject to $\boldsymbol{E}$ and $\boldsymbol{B}$ fields is given by:[14]

$$\mathrm{d}\boldsymbol{F} = \mathrm{d}q(\boldsymbol{E} + \boldsymbol{v} \times \boldsymbol{B}) \tag{1}$$

The torque about the center of mass on a body is defined as $\int_B \boldsymbol{r} \times \mathrm{d}\boldsymbol{F}$, where $\boldsymbol{r}$ points from the center of mass to the volume element. Using the differential force to find the net force and torque on a body gives:

$$\boldsymbol{F} = \int_B (\boldsymbol{E} + \boldsymbol{v} \times \boldsymbol{B}) \mathrm{d}q \tag{2}$$

$$\boldsymbol{L} = \int_B \boldsymbol{r} \times (\boldsymbol{E} + \boldsymbol{v} \times \boldsymbol{B}) \mathrm{d}q \tag{3}$$

If a body is rotating, the velocity relative to the magnetic field will vary over the body. Assuming an orbit inclined at 16°, the relative velocity at GEO is ∼1 km/s. If the body has a radius of 1 meter, and is rotating at 1 degree per second, the relative velocity from rotation is 10^{-5} times smaller than that from the orbit. In this analysis it is neglected.

Define the charge separation vector $\boldsymbol{q}$ and the total charge Q below to simply the force and torque:

$$Q = \int_B \mathrm{d}q \qquad \text{and} \qquad \boldsymbol{q} = \int_B \boldsymbol{r} \mathrm{d}q \tag{4}$$

Using the definitions in Eq. (4) in the integrals in Eq. (2) and (3) gives the following results for force and torque:

$$\boldsymbol{F} = (\boldsymbol{E} + \boldsymbol{v} \times \boldsymbol{B})\, Q \qquad \boldsymbol{L} = -(\boldsymbol{E} + \boldsymbol{v} \times \boldsymbol{B}) \times \boldsymbol{q} \tag{5}$$

Susceptibilities of AFM Parameters If the charge distribution were known at all times, Eq. (5) would be enough to predict force and torque, however, the charge distribution changes as the object rotates and charges or discharges. This subsection predicts the AFM parameters Q and $\boldsymbol{q}$ using the body voltage, ambient field $\boldsymbol{A}$, and two matrices found from the SMSM models discussed earlier.

If the voltage V is known, Q can easily be obtained through $Q = C_s\, V$ where C_s is the self capacitance, which can be found once using a commercial FEA tool as long as the objet does not change shape. The voltage on a spacecraft is a function of the solar flux, plasma environment, and the material properties of the spacecraft. There are many tools for predicting this voltage including analytical current balance methods as shown in Lai[16] or with computational tools such as NASCAP or SPIS.

Predicting the dipole is slightly more complex. The dipole can be thought of as the total charge Q multiplied by the separation of the center of charge from the center of mass. The charge will increase with the voltage, which will increase the magnitude of the dipole but not change the direction. An ambient field will push all the charge towards one end of the spacecraft. How far an ambient field is able to move the center of charge is dependent on the geometry and attitude of the spacecraft with respect to the ambient field. These two effects are lumped into the following equation:[11]

$$\boldsymbol{q} = \boldsymbol{\chi}_S V + [\chi_A] \boldsymbol{A} \tag{6}$$

Both of these susceptibilities ($\boldsymbol{\chi}_S$ and $[\chi_A]$) are found from SMSM models made with 100 spheres as shown in Fig. 2. The center of charge moves due to both the offset between center of mass and center of charge ($\boldsymbol{\chi}_S$) and the ambient field ($[\chi_A]$). In this analysis, offsets of centimeters are used which overwhelms the ambient effect. For example, this 10 cm plate charged to 30 kV with a $2\sqrt{2}$

cm offset in a Lorentz field created from a velocity of 1 km/s orthogonal to a 100 nT magnetic field will only see a charge-center movement of 7.7 pm. The torque produced by the center of mass offset is a much stronger (more than 9 orders of magnitude) than the torque created by the induced effect. Nonetheless, both effects are included.

$$\boldsymbol{F} = C_S V \boldsymbol{A} \tag{7}$$

$$\boldsymbol{L} = (\boldsymbol{\chi}_S V + [\chi_A]\boldsymbol{A}) \times \boldsymbol{A} \tag{8}$$

Note that $\boldsymbol{\chi}_S$ and $[\chi_A]$ are constants in the body frame much like the inertia tensor. Direction cosine matrices can be used to rotate $\boldsymbol{A}$ into the body frame or $\boldsymbol{\chi}_S$ and $[\chi_A]$ into whatever frame $\boldsymbol{A}$ is in to compute torque.

ORBITAL IMPACT CONSIDERING ONLY CHARGING

Charging combines with Earth's magnetic field to create an electrostatic force and torque. In this section, only the electrostatic force (Lorentz force) is considered from the perspective of orbital element changes and the maximum magnitude of acceleration, as torques have no direct effect on the orbital motion. Prior work has postulated if such Lorentz forces on their own could cause significant perturbations.[2] Thus, this section illustrates conservative estimates on the maximum perturbations that could be expected from natural charging. In this analysis a constant voltage of -30 kV is used, even though it will likely change with local time due to changing plasma conditions.

Gaussian Variation of Parameters

Gaussian variation or parameters are used to find the net impact of the Lorentz force. To find the mean secular rates of the orbital elements, integrate the rates with respect to time over one period. In a perfectly circular orbit this can be done analytically because $\nu = nt$, and Kepler's equation does not have to be solved. This is done for semi-major axis, eccentricity, inclination, and RAAN below. The argument of perigee rate is undefined for a circular orbit, and mean anomaly does not change observability.

$$\dot{a} = \frac{2}{n\sqrt{1-e^2}}\left(e\sin(\nu)a_R + \frac{p}{r}a_S\right) \rightarrow \Delta a = \int_0^P \frac{2}{n\sqrt{1-e^2}}\left(e\sin(nt)a_R + \frac{p}{r}a_S\right)\mathrm{d}t$$
$$= \frac{2P}{n\sqrt{1-e^2}}\frac{p}{r}a_S \tag{9}$$

$$\Delta e = \int_0^P \frac{\sqrt{1-e^2}}{na}\left[\sin(\nu)a_R + \left(\cos(\nu) + \frac{e+\cos\nu}{1+e\cos\nu}\right)a_S\right]\mathrm{d}t = 0 \tag{10}$$

$$\Delta i = \frac{1}{2\pi}\int_0^{2\pi} \frac{r\cos(\nu+\omega)}{na^2\sqrt{1-e^2}}a_W\,\mathrm{d}\nu = 0 \tag{11}$$

$$\Delta\Omega = \frac{1}{2\pi}\int_0^{2\pi} \frac{r\sin(\nu+\omega)}{na^2\sqrt{1-e^2}\sin(i)}a_W\,\mathrm{d}\nu = 0 \tag{12}$$

For a perfectly circular orbit, the only secular change is in the semi-major major axis, and is caused by an along-track acceleration. The Lorentz force cannot be in that direction, as the force

must act perpendicular to both the velocity and the magnetic field. Since the magnetic field at equatorial GEO points mostly north, the Lorentz force will be nominally in the radial direction. In reality no orbit is perfectly circular, and osculating changes to the elements can cause secular changes through feed back, but this simple analysis shows that a Lorentz force has no first-order impact on a circular orbit.

Acceleration Magnitude Analysis

In the earlier section, it is shown that there is no expected secular drift due to the Lorentz force for a circular equatorial GEO orbit. In this section the maximum accelerations caused by the Lorentz force are compared to other orbital forces. This provides an estimate of how much charging impacts osculating perturbations. Consider the example case of a charged aluminum sphere subjected only to the point mass gravity of the Earth, SRP, and the Lorentz force. For SRP, assume the cannonball model with full absorption. For the calculation of the Lorentz force, assume a magnetic strength of 100 nT, a velocity difference of 1 km/sec, and a voltage of -30 kV. The velocity difference comes from the orbit being inclined to 16°, as the magnetic field co-rotates with Earth, and -30 kV is a worst-case number. Gravity is calculated for geosynchronous altitude.

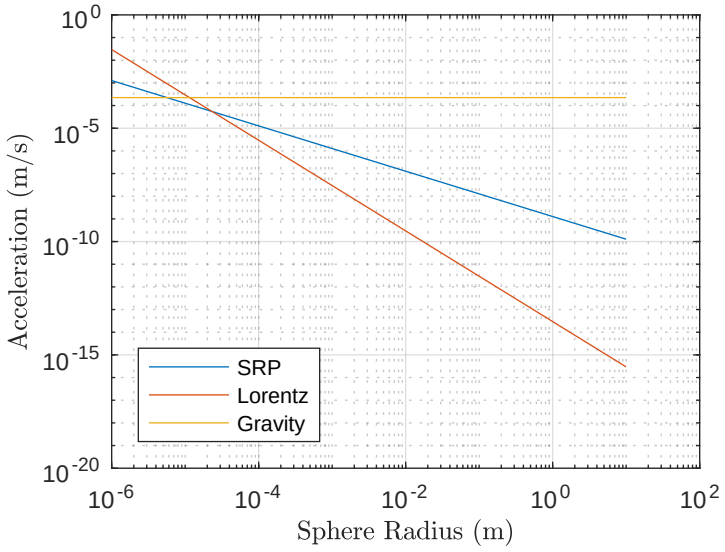

Figure 3. Accelerations of an aluminum sphere as a function of size

The acceleration of the aluminum sphere due to these three perturbations as a function of its size is shown in Fig. 3. As expected, the acceleration due to gravity is constant with respect to the object size. The force from SRP grows with the square of the radius, and the Lorentz force grows linearly with the radius, but the mass grows as the cube of the radius. This means that the SRP acceleration decays as $1/r$ while the Lorentz acceleration decays as $1/r^2$. Because of this, Lorentz forces are more significant when the object is small, as can be seen in Fig. 3. For the situation modeled here, charging is as significant as SRP for sphere with $r \sim 20\mu$m and charging is the dominant acceleration for spheres smaller than 10 μm. For larger spacecraft with $r \sim 1 - 10$m, gravity dwarfs SRP, which dwarfs charging. For more conservative charging levels, the sphere must be even smaller for charging to matter. This analysis shows that Lorentz forces only impact dust-sized object in a significant manner. For larger objects as spacecraft or spacecraft components such as torn-off

Mylar these electromagnetic forces are exceeding small and have a negligible impact. However, the impact of electromagnetic perturbations does not end here. The next section investigates the impact of electromagnetic torques along with other perturbations.

NUMERICAL PROPAGATION OF NOMINAL CASE INCLUDING CHARGING

Perturbations Considered

Numerous perturbations due to Earth, moon, sun solar pressure, electrostatics and Eddy current influence the orbits of HAMR objects at GEO. Each perturbation considered is detailed in Tab. 1 with either the exact equation or a short description.

Table 1. Forces and Torques acting on Space Debris

Perturbation	Force	Torque
Earth gravity	Spherical Harmonics up to 4th order	$\boldsymbol{L} = \frac{3\mu}{R_c^5}\boldsymbol{R}_c \times [I]\boldsymbol{R}_c$
Lunar gravity	point-mass gravity	0
Solar gravity	point-mass gravity	0
SRP	Absorptive, specular, and diffuse reflection	$\boldsymbol{L} = \boldsymbol{r}_{\text{sep}} \times \boldsymbol{F}_{\text{SRP}}$
Electrostatic	$\boldsymbol{F} = Q\boldsymbol{v} \times \boldsymbol{B}$	$\boldsymbol{L} = \boldsymbol{q}_{\text{sep}} \times (\boldsymbol{v} \times \boldsymbol{B})$
Eddy Currents	0	$\boldsymbol{L} = ([M](\boldsymbol{\omega} \times \boldsymbol{B})) \times \boldsymbol{B}$

Eddy current torque is included as well. When a conductor spins in a magnetic field, the mobile electrons move in loops because of induction. No net force is felt because the current path is closed, but an eddy current torque is felt. Gomez recently developed a general method for calculating this torque[17] through

$$\boldsymbol{L} = ([M](\boldsymbol{\omega} \times \boldsymbol{B})) \times \boldsymbol{B} \tag{13}$$

where $[M]$ is the magnetic tensor. For a flat plate, the matrix $[M]$ is given by

$$[M] = C_T \frac{\sigma e}{4} \boldsymbol{n}\boldsymbol{n}^T \tag{14}$$

where σ is the conductivity, C_T is a constant dependent on shape and size, and $\boldsymbol{n}$ is a unit vector normal to the plane. For a rectangle with length l greater than width w, C_T is found using St. Venant beam theory:

$$C_T \approx \frac{lw^3}{3(1 + 1.38(\frac{w^2}{l^2})^{1.6})} \tag{15}$$

in the cases considered, the normal axis of the plate is $\hat{\boldsymbol{z}}$ which makes the torque equal to

$$\boldsymbol{L} = ([M](\boldsymbol{\omega} \times \boldsymbol{B})) \times \boldsymbol{B} = C_T \frac{\sigma e}{4} (\omega_1 B_2 - \omega_2 B_1) \begin{bmatrix} B_2 \\ B_1 \\ 0 \end{bmatrix} \tag{16}$$

It is interesting to note that if the plate is spinning about its axis of maximum inertia, ω_3 will be large and ω_1 and ω_2 will be small or zero. The eddy torque will also be small, and the object's spin will be relatively unaffected. If the object is tumbling, only the spin rates about the body 1 and 2 axes are removed and it will eventually fall into a stable spin about its axis of major inertia.

The magnitude of the SRP force is determined by the solar flux and the illuminated area. The direction is governed by the amount of light that is absorbed and reflected specularly and diffusely. The SRP force is given by:[18]

$$\boldsymbol{F} = p_{SRP} A \cos(\theta) \left[\rho_A \hat{\boldsymbol{s}} + 2\rho_s \cos(\theta) \hat{\boldsymbol{n}} + \rho_d (\hat{\boldsymbol{s}} + \frac{2}{3} \hat{\boldsymbol{n}}) \right] \tag{17}$$

Where θ is the angle between the sun-pointing line and the face normal, $\hat{\boldsymbol{s}}$ is the sun-pointing vector, $\hat{\boldsymbol{n}}$ is normal to the plane, and $\rho_A, \rho_S,$ and ρ_D are the absorptive, specular, and diffuse coefficients, respectively, which must sum to unity.

Magnetic Field Models

Earth's magnetic field at low altitudes is well approximated by the IGRF model, which takes many factors affecting Earth's geodynamo into account. Outside Earth's magnetosphere, the magnetic field is purely a function of space weather and has little to no dependance on Earth's own magnetic field. At GEO, these two effects combine to make a complex function of time and space weather parameters. The current state of the art for modeling this field is the Tsyganenko model.[19] There have been many versions and updates to this model, but in this analysis the 2001 version is used with GEOPACK 2008* for coordinate transforms.

Since the magnetic field is position dependent, the model is run at each timestep. The time is assumed to be January 1, 2002, midnight, for all runs. The space weather parameters used are shown in Tab. 2, and are representative values that are used by the Community Coordinated Modeling Center (CCMC) on their single-run website†

Table 2. Space weather parameters used for Tsyganenko model

Parameter	Value
Solar Wind Dynamic Pressure	4 nPa
Solar Wind Velocity	400 km/s
IMF B_y	6 nT
IMF B_z	-5 nT
DST	-30 nT

This produces a magnetic field model that accounts for the solar wind and Earth's geodynamo. As shown in Fig. 4, the field is not well-modeled by a tilted dipole alone. The x and y axes are in earth radii, and the z axis is arbitrary. Space weather will have a dramatic effect on the charging and the magnetic field strength and direction. Solar storms can cause high charge levels and cause strong electric and magnetic fields.[15] Since these fields are short-lived and oscillatory, the subsequent electrostatic perturbations are not directly capable of causing dramatic orbital changes. However, they may cause shape changes which may then change the orbit. For instance, consider a flexible sheet of conducting mylar, which when uncharged is wadded into a small ball. If it suddenly charges from +10 V to -10 kV due to a solar storm, it may inflate and change its area by a factor of 10 or 100. This would dramatically affect the SRP force and torque which would dramatically affect the orbit.

*http://ccmc.gsfc.nasa.gov/modelweb/magnetos/tsygan.html

†http://ccmc.gsfc.nasa.gov/requests/instant/tsyganenko.php

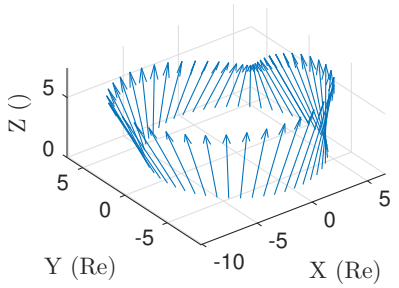

Figure 4. ECI Magnetic field used in this study, Z axis is arbitrary

The voltage of a conducting sheet is perhaps one of the easier spacecraft charging problems one could pose, nonetheless it is a still a hard problem. The voltage was modeled under very harsh charging conditions by Früh et al. in Reference 6 for a sheet with one side conducting and one of different dielectrics such as Kapton and Mylar. The most extreme voltage found was slightly more negative than -30 kV and occurred when using the very high ATS-6 flux. In this analysis, a simple and constant value of -30 kV is used to give a rough maximum for the charge level. In many circumstances, the voltage would be much smaller.

Self Capacitance Estimation for Rectangular Plates

Calculating the self capacitance of a square plate is a well-studied problem. J.C. Maxwell himself estimated it to be 0.40 pF for a 1 cm square,[20] and current computation methods now estimate it at 0.4019 pF.[21] The self capacitance of two geometrically similar objects, will scale linearly with any dimension. For instance, the self capacitance of a sphere is given by $C = 4\pi\epsilon_0 R$. For a flat plate, capacitance can be expressed as $c = C/B$ where C is the true capacitance in Farads, and B is the bigger side of the plate. For a square plate B is just the edge length.

Reitan and Higgins[22] produced a very useful curve from which c can be extrapolated from the aspect ratio of the big to small side B/S. Ten points are read off this curve, and a power law is used to fit it with good accuracy ($r^2 = 0.9995$). The power law is shown below.

$$c = \left(0.402 * 10^{-10} \frac{\mathrm{F}}{\mathrm{m}}\right)\left(\frac{B}{S}\right)^{-0.4733} \tag{18}$$

The capacitance is used to convert the voltage, which can often be estimated from space weather parameters and is assumed to not depend on size or shape, to the charge. The amount of charge will dictate the magnitude of the force.

Numerical Propagation of Nominal Case

A nominal case of a thin rigid square of mylar is considered first. The material parameters are shown in Tab. 3. The inertia tensor is computed assuming constant density. The center of charge is separated from the center of mass by $\boldsymbol{r}_{\mathrm{CC}}$ while the center of pressure, which is used for SRP, is separated from the center of mass by $\boldsymbol{r}_{\mathrm{CP}}$. Any matrix values not explicitly defined are zero.

Four different models are used to propagate the orbit of the plate. The longitude and altitude departure over time are shown in Fig. 5. Model 1 is the full model, model 2 neglects electrostatic force and torque, model 3 additionally neglects eddy torques, and model 4 additionally neglects

Table 3. Nominal HAMR propagation values[6,23]

Parameter	Value
thickness	1/4 mil (6.35 μm)
density	1.39 g/cm^3
L_x	10 cm
L_y	10 cm
C	4.02 pF
$\boldsymbol{r}_{\text{CC}}$	$[2,2,0]^T$ cm
$\boldsymbol{r}_{\text{CP}}$	$[2,2,0]^T$ mm
$\boldsymbol{\chi}_S$	$80.43 * [1,1,0]^T$ fF m
$\chi_A(1,1)$	$5.393 * 10^{-11}$ F m^2
$\chi_A(2,1), \psi_A(1,2)$	$1.711 * 10^{-14}$ F m^2
$\chi_A(2,2)$	$1.613 * 10^{-12}$ F m^2
ρ_A	0.5
ρ_S	0.2
ρ_D	0.3
σ_C	3.5*10^7 S/m
$M_{3,3}$	333.12 Sm^4

attitude-dependent SRP and uses a cannonball model. The orbits for each of these propagators all start at the same place, with no altitude departure and 241° longitude. By the end of the 48 hour propagation, the full model predicts a location that is 1441 km away from the model that neglected only statics, 2351 km away from the model that neglected statics and eddy torques, and 3354 km away from the model that neglected all electromagnetic effects and used cannonball SRP.

The Gaussian variation of parameters analysis shows that electrostatic forces can only affect the orbit by a few tens of meters per orbit, yet Fig. 5 shows thousands of kilometer departures caused by including electrostatic and eddy effects. To investigate how such small forces and torques can cause such a drastic change in the orbital position, the magnitudes of the linear and rotational accelerations are now investigated. For the full propagator model, the norm of the linear and rotational accelerations are shown in Fig. 6.

As is expected for a circular orbit, the linear acceleration from Earth's gravity stays constant. The SRP acceleration is heavily attitude dependent and changes magnitude quickly as the plate tumbles, but is still by far the largest perturbation. Solar and Lunar gravity change slowly as the distance to the plate changes. The electrostatic force is the smallest by many orders of magnitude.

As for the torques SRP is still the largest, but is followed more closely by electrostatic and eddy torques while gravity gradients are many orders of magnitude smaller. Electrostatic and eddy torques cause rotational accelerations near 1 Radian per hour^2, which means that in one hour they could change the attitude by 1/2 a radian if they acted in the same direction using $\Delta\theta = \frac{1}{2}\ddot{\theta}\Delta t$. This is the key to how electrostatic and eddy effects can change an orbit so drastically — over time periods longer than a few hours, electrostatic and eddy torques can significantly change the attitude of a HAMR object, which changes SRP, which changes the orbit.

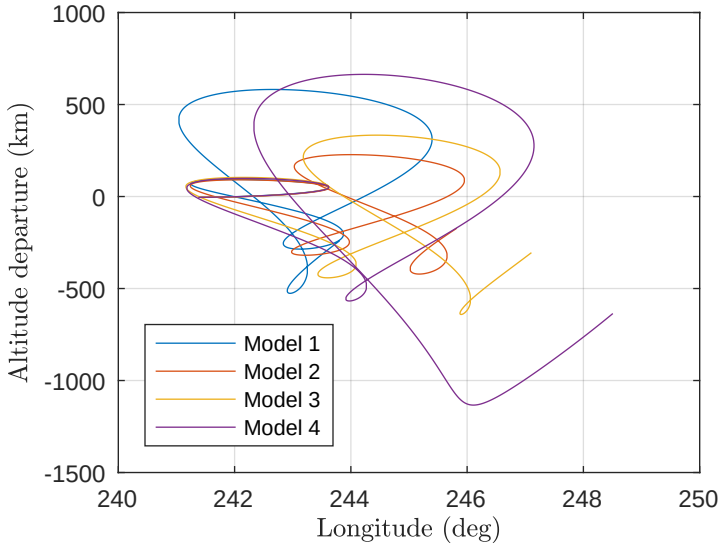

Figure 5. Longitude and altitude for plates with different propagation models

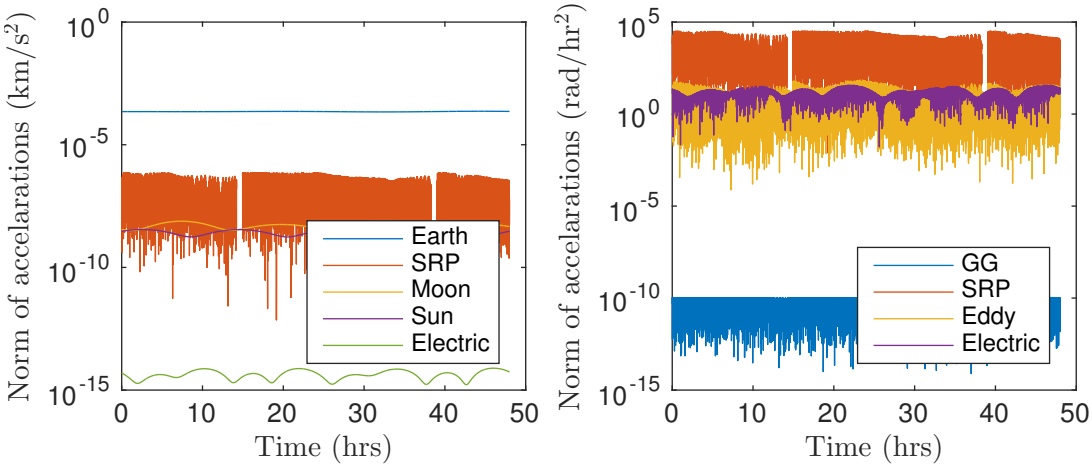

(a) Linear Accelerations

(b) Angular Accelerations

Figure 6. Accelerations for charged HAMR object during propagation

This matches the findings of other authors as well. Früh et al[6] found that including eddy torques for a thin HAMR object caused major orbital differences, but Paul et al.[7] modeled a sphere for which torques do not act and found minimal orbital differences. The Lorentz force cannot change the orbits of objects large enough to be observable. However electrostatic and eddy torques can change the attitude, and if the attitude influences SRP, the orbit can be measurably changed.

Monte Carlo Analysis over Initial Attitude

Attitude makes a large difference in the final position of a HAMR object. This begs the question of whether the thousands of kilometers differences that come from including or neglecting electromagnetic effects are larger or smaller than the normal spread from initial attitude. Put more mathematically, assuming a distribution of initial attitudes, are the differences in the means of the distribution of final positions when including or neglecting electromagnetic effects significant when compared with the standard distribution of either population?

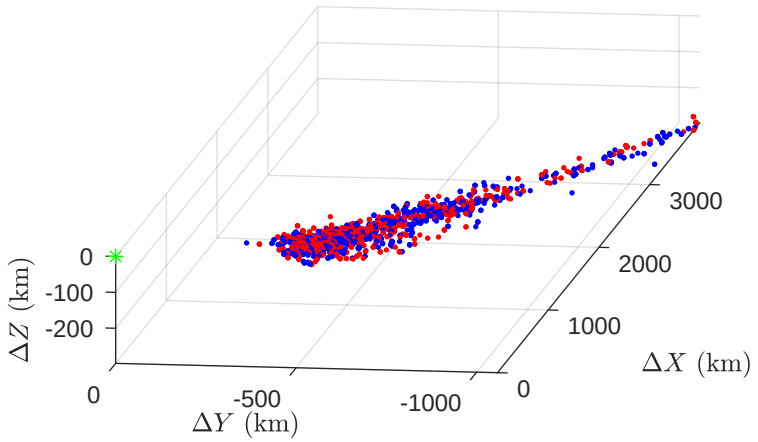

Figure 7. Final positions after of HAMR objects at GEO after 24 hour propagation including or neglecting electromagnetic effects

To answer this question, the initial attitude of the plate is randomized in a Monte Carlo analysis, and propagated with models that either include electromagnetic effects (electrostatic force and torque as well as eddy torques). One thousand initial attitudes are propagated for 24 hours and the final position and velocities for both models are stored in a master file. The final ECI positions are shown in Fig. 7. The red dots represent plates that were propagated including electromagnetic effects, and the blue dots represent plates that were propagated neglecting these effects. The green point is the original position, where all points would lie if a two body propagator is used for this 24 hour propagation. The distances on the axes are given relative to the original position, and are in the ECI coordinate system.

The spread for either population is thousands of km in the along-track direction, which is comparable to the differences found with different propagation models in Fig. 5. The mean and standard deviation of the ECI positions for both the populations propagated with and without electromagnetic effects, and are compared against each other. The differences in the means is divided by the standard

deviation in the positions of the population propagated without electromagnetic effects and is shown below. Dividing by the standard deviation of the charged population gives very similar results.

$$\Delta\mu_X = -0.205\,\sigma_X \qquad \Delta\mu_Y = 0.219\,\sigma_Y \qquad \Delta\mu_Z = 0.237\,\sigma_Z \tag{19}$$

The difference in the means is a significant fraction of the standard deviation when randomizing initial attitude, which suggests that including electromagnetic effects does change the orbits of uncontrolled HAMR objects beyond their normal spread. To further investigate this, the classical orbit elements are computed for both populations at the end of the propagation period. The final distributions are shown for both the propagation models.

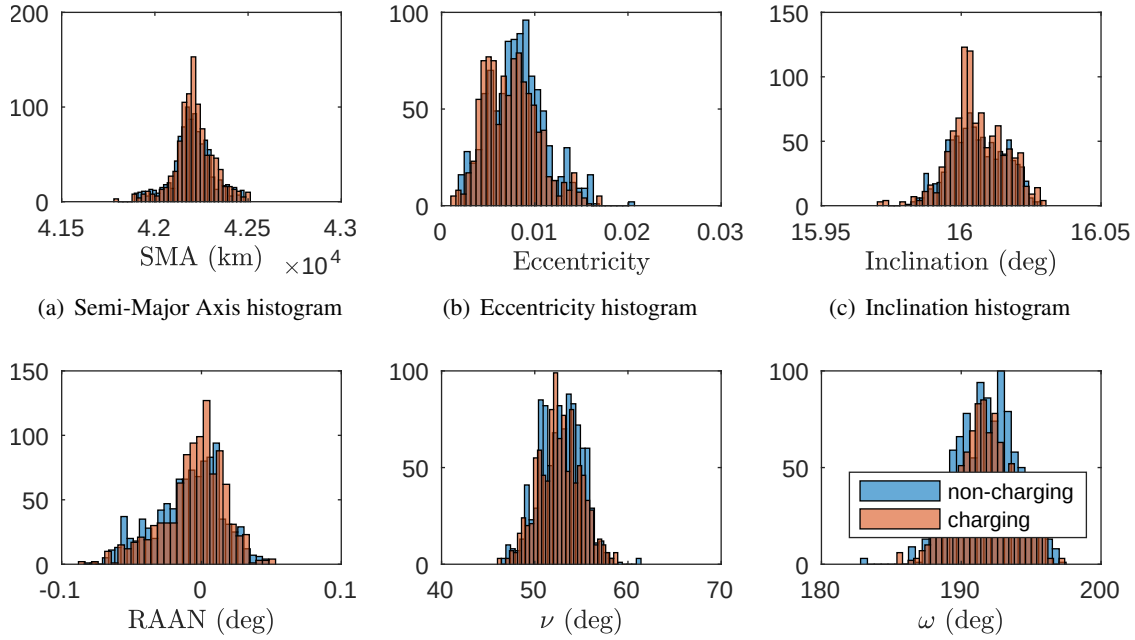

(a) Semi-Major Axis histogram

(b) Eccentricity histogram

(c) Inclination histogram

(d) Right Ascension of Ascending Node histogram

(e) True Anomaly histogram

(f) Argument of Perigee histogram

Figure 8. Histograms of classical orbit elements for charging and non-charging propagation

There are many interesting observations to make from these histograms. Firstly, the spread in all elements after only 24 hours or propagation is very large. All angular elements except inclination and RAAN have at least 10° of spread after only 24 hours, and the semi-major-major axis changes by hundreds of kilometers. The eccentricity and RAAN visually seem to have different populations stemming from different propagators. To test the probability that including electromagnetic effects have no significant effect, hypothesis testing is used. A truth test is used to compute the probability that both sample sets (from using different propagation models) come from the same actual population and any apparent differences would disappear with enough samples. This probability is shown in Tab. 4 along with whether the orbital element is effected by electromagnetic effects applying a 5% probability threshold.

Eccentricity and RAAN have vanishing probabilities of not being effected, and semi-major major axis has a very small one. This means that including electromagnetic effects such as Lorentz forces and torques as well as eddy torques makes a significant difference even when randomizing the

Table 4. Hypothesis testing for effect of electromagnetic effects

Orbital Element	Probability of no Effect	Affected?
Semi-Major Axis	1.96 %	Yes
Eccentricity	9.97e-7 %	Yes
Inclination	76.2%	No
True Anomaly	21.1%	No
RAAN	4.24e-4 %	Yes
Argument of Perigee	44.6%	No

initial attitude of the plate. For the example case of an extremely lightweight metallic sheet at -30 kV, including electromagnetic effects is necessary for accurate propagation. The next section will investigate whether electromagnetic effects are as important for other objects and scenarios.

COMPARISON OF TORQUES FOR GENERAL OBJECTS

SRP is the driver for HAMR objects, but it can be steered by electromagnetic torques. This section investigates what objects are susceptible to such electromagnetic torques. First consider the same 10 cm square plate considered in previous analysis, but allow the voltage to vary. If the plate is uncharged electrostatics will no longer act, and earlier analysis shows that at -30 kV it does matter, but is there a charging threshold where electrostatics begin to contribute? To answer this question, the voltage of the plate is varied logarithmically from 10 Volts, which is a normal floating potential, to 100 kV, which is slightly higher than the worst case charging ever modeled.[24] The plate's orbit is propagated for 24 hours, and the torques are recorded. The angular acceleration that the plate experiences due to each perturbation is shown in the log-log plot in Fig. 9. The linear accelerations are not shown because the orbit change comes from electromagnetic torques reorienting the plate which changes SRP.

Since all of the torques are attitude dependent, they vary quickly through time as the plate tumbles. To give a sense of the normal variation, the mean and 1-σ bounds are shown. Because many of the torques are logarithmically distributed, the standard deviation is larger than the mean, and does not apply for a non-symmetric distribution. Rather, the logarithms or the angular accelerations are used to make the statistics, then exponentiated for plotting. This is shown below:

$$x' = \log(x) \rightarrow \quad \bar{x} = 10^{\bar{x'}} \tag{20}$$

$$\rightarrow \bar{x} \pm \sigma_x = 10^{\bar{x'} \pm \sigma_{x'}} \tag{21}$$

The torques from gravity gradients, SRP, and eddy currents are all relatively constant with voltage, which would be expected. However, the torque from electrostatics rises steadily. If 1 radian is used as an arbitrary marker of a significant attitude change, the time scales on which electrostatics will act can be investigated. For 10 Volts, the mean angular acceleration is 3.5e-3 Rad/hr^2. Using $\Delta\theta = \frac{1}{2}\ddot{\theta}\Delta t^2$ gives a time scale of 23.8 hours. At 600 Volts, the time needed for significant attitude perturbations is 3 hours, and at 100 kV it only takes 14 minutes. Of course this assumes the torque is always about the same body axis, which is not always true but gives a convenient upper bound.

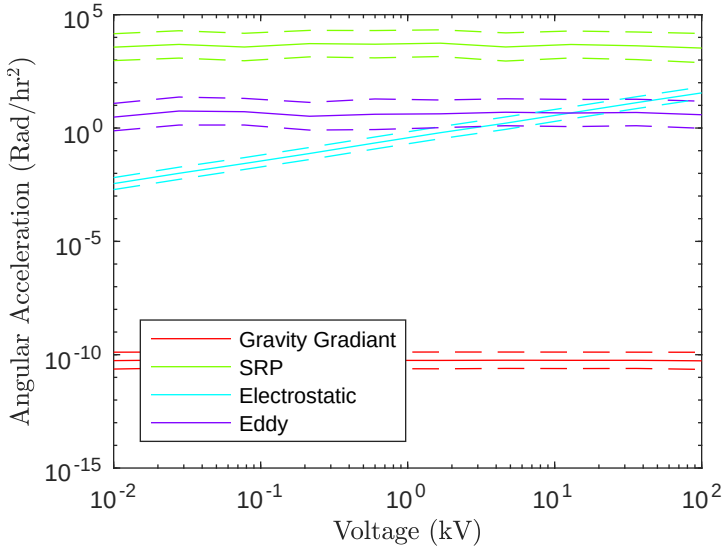

Figure 9. Angular accelerations due to various perturbations at different voltages

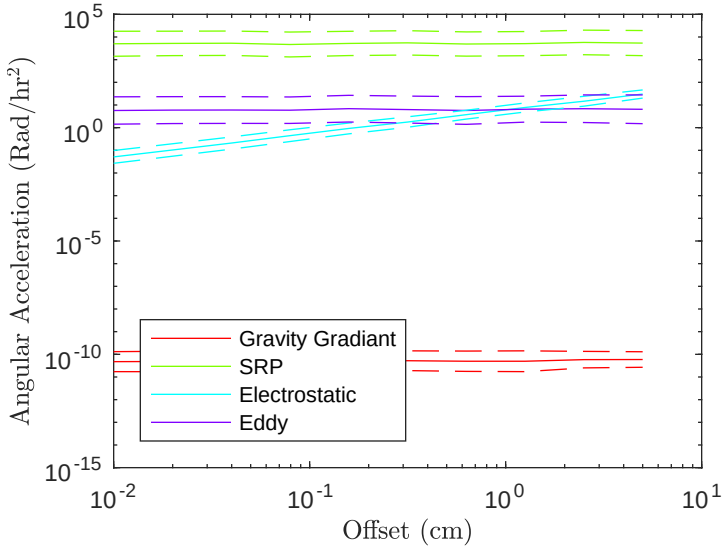

Figure 10. Angular accelerations due to various perturbations at different CM offsets

This same analysis is repeated varying not voltage but the separation between center of charge and center of mass while the voltage is fixed at 30 kV in Fig. 10. Once again all perturbations except electrostatics are relatively constant, while electrostatic torques grow with the separation, as this lengthens the moment arm. Electrostatics become larger than eddy currents for all offsets larger than 1 cm on this 10 cm square plate, although the variance associated with eddy currents is much larger. Once again using 1 radian as a threshold for significant attitude perturbations that could influence the orbit gives timescales on which charging can act. At 0.1 mm of offset, electrostatic torques will take nearly 6 hours to significantly change the attitude, at 1.5 mm, the timescale is 1.5 hours, and at 5 cm (half the length of the plate), electrostatics have a timescale of only 16 minutes.

Next consider the same thin 10 cm sheet but hold the voltage, separation of center of charge and center of mass, and thickness constant, but allow the initial spin to vary. The initial spin in all prior work is set to zero, but in this section the stability of spinning about an axis of maximum inertia is considered. Intuitively, a frisbee or football will be less susceptible to small torques that would otherwise cause it to tumble if it were spinning faster. Likewise, the thin plate will be less susceptible to small electromagnetic torques if it were spinning stably about its axis of maximum inertia, which is the body z axis.

To study this, consider a plate spinning like a frisbee about its z axis at a rate of ω_0. Apply a torque about the body x axis of $L_x = \chi_S V B \Delta v = (1.1376{*}10^{-13}$ C m$)(30\text{kV})(100\text{nT})(1\text{km/s}) = 3.4127 * 10^{-13}$ Nm for one hour, then propagate normally for another hour. The angle between the body z axis and the inertial z axis (which are aligned at the beginning of the simulation) is plotted below in Fig. 11 for a fast initial spin ($\omega_0 = 2^\circ/s$) and a slow initial spin ($\omega_0 = 0.1^\circ/s$). Keep in mind that with no initial spin, this problem becomes 1 dimensional, and after one hour of torque the place should have rotated by $\Delta\theta = \frac{1}{2}\frac{L_x}{I_x}\Delta t^2 = 1723^\circ$, nearly 5 entire rotations.

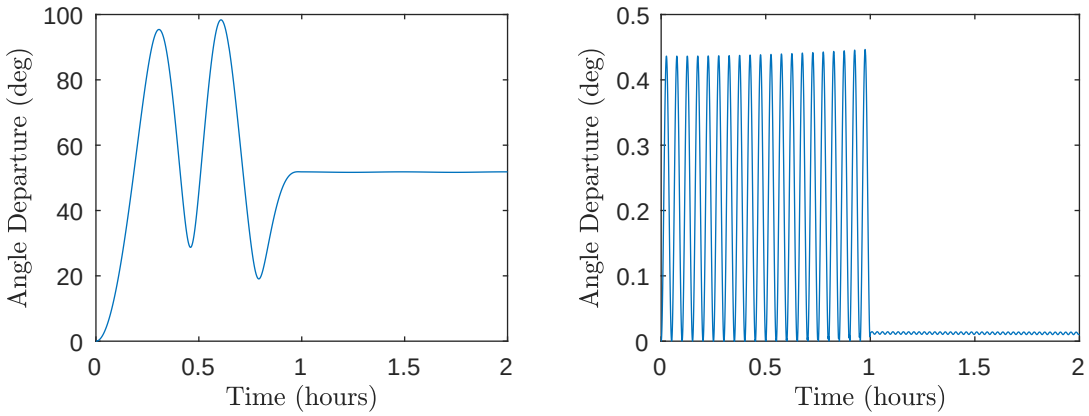

(a) Slow initial spin – $\omega_0 = 0.1^\circ/s$

(b) Fast initial spin $\omega_0 = 2^\circ/s$

Figure 11. Departure from initial sun-pointing angle due to electrostatic torques

From this simple example the importance of initial spin can be seen dramatically. If the initial spin is a slow 0.1 degrees per second, one hour of electrostatics can change the body attitude, which changes SRP, by 50 degrees. If the initial spin is increased to 2 $^\circ$ per second, the same electrostatic torque only changes the sun pointing angle by a mere 0.01 degrees. Clearly objects spinning stably about the axis of maximum inertia are less susceptible to small electrostatic or eddy torques. As an aside, eddy torques never act about the z axis for plates of vanishing thickness, so they are not able

to change the attitude, and therefore the orbits, of thin plates spinning about their maximum inertia axis.

To further investigate the trend illustrated above where objects spinning stably are less susceptible to small torques, vary the initial spin logarithmically from 0.01 to 10 degrees per second and monitor the attitude departure. The attitude is monitored by computing the mean and standard deviation of the angle between the body and inertial z axis in the second hour, after the electrostatic torque has been turned off. This is shown in Fig. 12

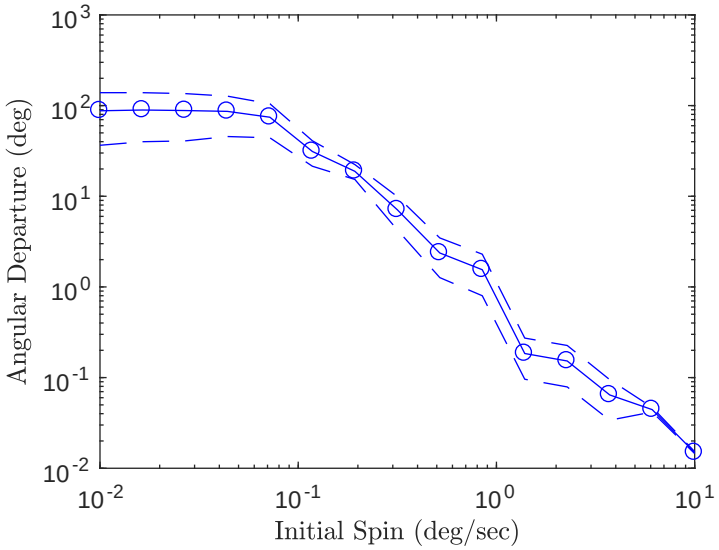

Figure 12. Influence of initial spin on attitude departure

The mean attitude departure in the second hour is shown as the solid line with the circles and the dashed lines show the 1-σ bounds. When the plate has a low initial spin, (0.01 - 0.1 $^\circ$/s per second), the departure is a nearly flat line, because the body z axis can never be more than 180° from the inertial z axis. For higher initial spin rates ($\omega_0 > 0.1$ $^\circ$/s per second), the departure angle drops quickly. Choosing again the arbitrary marker for significant attitude change of 1 radian ($\sim 57^\circ$) gives a cutoff spin rate past which electrostatic torques may not have as much influence on the orbit of 0.085 $^\circ$/s per second.

Keep in mind that in this simulation the electrostatic torque is assumed to act completely in the body x axis and be constant. This is not likely in the full coupled problem. Additionally, these results hold only for the 10 cm by 10 cm by 1/4 mil sheet of mylar charged to 30 kV. Heavier and less dramatically charged objects will require smaller stable initial spins to overwhelm the electrostatic torques.

For the thin cases considered earlier, SRP is very sensitive to attitude – if the plate is directly facing the sun the acceleration is thousands of times larger than if the plate faces orthogonal to the sun. For a cube, the attitude only changes the exposed area by a factor of 2 or 3. This shows that objects like plates with highly attitude-dependent cross-sectional are more susceptible to the small torques caused by electrostatics and eddy currents. Additionally this heavier object will be less susceptible to non-gravitational perturbations like electrostatics and SRP.

To explore this, consider the same 10 cm square of Mylar, but allow the thickness to vary from the very thin 1/4 mil (6.35 μm) to 10 cm which turns the sheet into a solid cube of Mylar. As this 10 cm cube weighs 1.39 kg, this is a good approximation of a cubesat. Each of the sheets are propagated for 24 hours, and the linear and angular accelerations are recorded at each time, much like the results shown in Fig. 6. The mean and standard deviation are computed for the time-series of the accelerations for each plate thickness and are plotted in Fig. 13. The means are plotted as solid lines, and the $1-\sigma$ bounds are shown as dashed lines. In some cases the standard deviation is larger than the mean, and the lower bound of the norm is negative and does not appear on this log plot.

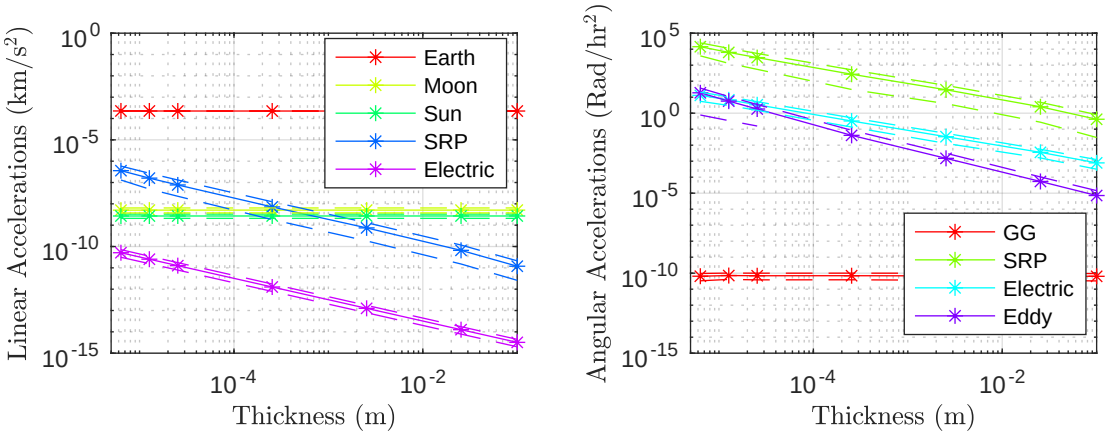

(a) Linear Accelerations

(b) Angular Accelerations

Figure 13. Acceleration on plates of varying thickness from different perturbations

There are many interesting trends in both plots. Considering linear accelerations, the gravitational accelerations are constant with object size. This is expected as mass divides out of the gravitational formula. The non-gravitational accelerations (Lorentz force and SRP) decrease as the plate gets thicker because the force stays roughly constant (the full 3-dimensional SRP calculation is performed, but the self capacitance is assumed to stay constant even though the plate becomes thicker). The Lorentz force is consistently the smallest perturbation, and is nearly 10,000 times smaller than SRP. This will not have a large effect on propagation. For the angular accelerations, gravity gradient accelerations remain constant, as both the torques and the inertia increase as the plate gets thicker. All other accelerations become smaller because of the increasing inertia. SRP is the largest torque, but is followed by electrostatics and eddy torques. Eddy torques have a more negative slope than electrostatics – this is an indirect effect due to the thicker plates spinning up to lower rates, which causes the eddy torques to decrease.

For large heavy objects, the torques will take much longer to change the attitude and "steer" SRP. Furthermore, these objects will not change their exposed areas as much due to rotations, which further suppresses the orbital effects of electromagnetic torques. For small lightweight objects, the small electromagnetic torques can drastically change the orbit by changing the attitude.

CONCLUSION

There are many perturbations which influence the orbit of GEO objects. This paper develops the models needed to include electrostatic perturbations for GEO objects, investigates how these

perturbations change the orbit, and analyzes the objects and orbit scenarios where electrostatic and eddy perturbations will be the most significant and ought to be considered.

For a spherical object, the Lorentz force it is insignificant for objects larger than 100 μm in diameter, as gravity and SRP dominate. For non-spherical objects, the weak torques from electrostatic and eddy effects can change the attitude, which changes the strong perturbation of SRP. This allows the weak electromagnetic perturbations to steer the strong SRP perturbation and change the orbits of objects large enough to be observed. Including these electromagnetic effects can change the final position after 2 orbits by thousands of kilometers, and cause significant differences in a 24 hour Monte Carlo over initial attitude.

The objects that are the most susceptible to these small electromagnetic torques is investigated by comparing to a nominal HAMR sheet of Mylar charged to 30 kV, having a 2.82 cm offset between the center of mass and center of charge, and no initial spin. Holding all else constant, electrostatics will begin to significantly contribute for voltages higher than a kilovolt, or separations larger than a millimeter. Even if these small electromagnetic torques can change the attitude in a short time, this will only translate to large orbit changes if the area exposed to SRP changes dramatically because of this attitude change as it does for a thin plate. The inertia and mass also change as the thickness of a plate grows, and increase the time needed for electromagnetic torques to take effect. Lastly the initial spin rate about a stable axis is found to reduce the effect of electrostatics. For the object considered here, spins faster than 0.1 $^\circ/$s per second are found to overwhelm electrostatics on the time period of an hour.

From this, it is concluded that electrostatics can significantly impact the orbits of some objects. Likely candidates for which charging will matter are either tiny objects for which the Lorentz force will contribute, or thin sheets where small electrostatic and electromagnetic torques can "steer" SRP. For these small torques to matter, the object must be highly charged, have its center of charge offset from its center of mass, and not be spinning quickly about a stable axis.

REFERENCES

[1] T. Schildknecht, R. Muscia, M. Plonera, G. Beutlera, W. Fluryb, J. Kuuselac, J. d. Leon Cruzd, and L. d. Fatima Dominguez Palmerod, "Optical observations of space debris in GEO and in highly-eccentric orbits," *Advances in Space Research*, 2004, pp. 901–911.

[2] W. E. Wiesel, "Estimating Nongravitational Accelerations on High Area to Mass Ratio Objects," *Journal of Guidance, Control, and Dynamics*, Vol. 0, Feb. 22 2015.

[3] T. Schildknecht, R. Musci, C. Frueh, and M. Ploner, "Color Photometry and Light Curve Observations of Space Debris in GEO," *Procedings of the Internaitonal Astronautical Congress*, 2008.

[4] J. A. Dever, K. K. d. Groh, J. A. Townsend, and J. A. Townsend, *Mechanical Properties Degradation of Teflon FEP returned from the Hubble Space Telescope*. American Institute of Aeronautics and Astronautics, 1998.

[5] J. F. Fennell, H. C. Koons, M. Leung, and P. Mizera, "A review of SCATHA satellite results: Charging and discharging," *1983.*, 1983, pp. 3–11.

[6] C. Früh, D. Ferguson, C. Lin, and M. Jah, "The Effect of Passive Electrostatic Charging on Near-Geosyncronous High Area-To-Mass Ratio Objets," *International Astronautical Congress*, Vol. 64, 2013.

[7] S. N. Paul and C. Frueh, "Space Debris Charging and its Effect on Orbit Evolution," *AIAA/AAS Astrodynamics Specialist Conference*, Long Beach, CA, American Institute of Aeronautics and Astronautics, 13-16 September 2016.

[8] J. Hughes and H. Schaub, "Charged Geosynchronous Debris Perturbation Using Rapid Electromagnetic Force and Torque Evaluation," *Advanced Maui Optical and Space Surveillance Technologies Conference*, 2016.

[9] D. Stevenson and H. Schaub, "Multi-Sphere Method for Modeling Electrostatic Forces and Torques," *Advances in Space Research*, Vol. 51, Jan. 2013, pp. 10–20, 10.1016/j.asr.2012.08.014.

[10] D. Stevenson, "Optimization of Sphere Population for Electrostatic Multi Sphere Model," *12th Spacecraft Charging Technology Conference*, Kitakyushu, Japan, May 14–18 2012.

[11] J. Hughes and H. Schaub, "Appropriate Fidelity Electrostatic Force Evaluation Considering a Range of Spacecraft Separations," *AAS/AIAA Spaceflight Mechanics Meeting*, Feb. 14–18 2016.

[12] S. Price, A. Stone, and M. Alderton, "Explicit formulae for the electrostatic energy, forces and torques between a pair of molecules of arbitrary symmetry," *Molecular Physics*, Vol. 52, No. 4, 1984.

[13] D. C. Giancoli, *Physics for Scientists and Engineers*. Pearson Prentice Hall, 2008.

[14] D. J. Griffiths, *Introduction to Electrodynamics*. Prentice Hall, 3rd ed., 1999.

[15] D. M. Malaspina, J. R. Wygant, R. E. Ergun, G. D. Reeves, R. M. Skoug, and B. A. Larsen, "Electric field structures and waves at plasma boundaries in the inner magnetosphere," *Journal of Geophysical Research (Space Physics)*, Vol. 120, 2015, pp. 4246–4263.

[16] S. T. Lai, *Fundamentals of Spacecraft Charging: Spacecraft Interactions with Space Plasmas*. Princeton University Press, 2011.

[17] N. Ortiz Gomez and S. J. I. Walker, "Eddy Currents applied to de-tumbling of space debris: feasibility analysis, design and optimization aspects," *Acta Astronautica*, Vol. 114, 2015, pp. 34–53.

[18] B. Wie, *Space Vehicle Dynamics and Control*. Reston, VA: AIAA Education Series, 2nd ed., 2008.

[19] N. A. Tsyganenko, "A Magnetospheric magnetic field model with a warped tail current sheet," *Planetary and Space Science*, Vol. 37, 1989, pp. 5–20.

[20] J. Maxwell, *A Treatise on Electricity and Magnetism*. Oxford University Press, 1893.

[21] D. N. D. G. Allen and S. C. R. Dennis, "The Application of Relaxiation Methods to the Solution of Differential Equations in Three Dimensions," *Quarterly Journal of Mechanics and Applied Mathematics*, Vol. 6, 1953, p. 87.

[22] D. K. Reitan and T. J. Higgins, "Accurate Determination of the Accurate Determination of the Capacitance of a Thin Rectangular Plate," *Transactions of the American Institute of Electrical Engineers, Part I: Communication and Electronics*, Vol. 75, No. 6, 1957, pp. 761–766.

[23] J. McMahon and D. J. Scheeres, "A New Navigation Force Model for Solar Radiation Pressure," *AIAA Journal of Guidance, Control and Dynamics*, Vol. 33, 2010, pp. 1418–1428.

[24] D. C. Ferguson, W. F. Denig, and J. V. Rodriguez, "Plasma Conditions During the Galaxy 15 Anomaly and the Possibility of ESD from Subsurface Charging," *AIAA Aerospace Sciences Meeting including the New Horizons Forum and Aerospace Exposition*, Orlando, FL, January 4–7 2011. Paper AIAA 2011-1061.